Key Engineering Materials
ISSN: 1662-9795, Vol. 1022, pp 69-76
doi:10.4028/p-M8r40M

Submitted: 2024-09-19
Accepted: 2025-05-05
Online: 2025-09-08

DFT Calculations on the Termination of 4H-SiC Non-Polar Surfaces during Photoelectrochemical Pore Formation

Tingqiang Yang[1,2,a*], Marco Perazzi[1,2,b], Christopher Zellner[1,2,c], Georg Pfusterschmied[1,2,d], Ulrich Schmid[1,e]

[1]Institute of Sensor and Actuator Systems, TU Wien, Gusshausstrasse 27-29, 1040 Vienna, Austria

[2]Christian Doppler Laboratory for Sustainable Silicon Carbide Technology, Gusshausstrasse 27-29, 1040 Vienna, Austria

[a]tingqiang.yang@tuwien.ac.at, [b]marco.perazzi@tuwien.ac.at, [c]christopher.zellner@tuwien.ac.at, [d]georg.pfusterschmied@tuwien.ac.at, [e]ulrich.e366.schmid@tuwien.ac.at

Keywords: Porous 4H-SiC, surface termination, PECE, DFT.

Abstract. In our previous work, single-crystalline porous 4H-SiC thin foils were successfully released from a monocrystalline 4H-SiC wafer by photoelectrochemical etching (PECE). This technology is promising for the next-generation power device fabrication processes (*e.g.* cost-efficient engineered substrates) and micro-electromechanical systems. The surface terminations of the pore walls will affect the behavior in the further fabrication process and application, thus motivating the need for detailed investigations. This work based on DFT calculations focuses on the surface terminations of five 4H-SiC non-polar surfaces, *i.e.* $\{10\bar{1}0\}$, $\{11\bar{2}0\}$, $\{21\bar{3}0\}$, $\{31\bar{4}0\}$ and $\{32\bar{5}0\}$, which can well represent the walls of the C-face etched pores penetrating through the released foil along the [0001] direction. The surface energies of the stoichiometric surfaces are found to be in the sequence of $\{11\bar{2}0\} < \{32\bar{5}0\} < \{21\bar{3}0\} < \{10\bar{1}0\} < \{31\bar{4}0\}$. All these surfaces have high chemical affinity to H_2O and even more to HF. In particular, for the complete surface termination by HF, the relative stability of these crystal planes can be changed and depends on the HF chemical potential. For example, in the range of HF chemical potential from −4.10 to −1.70 eV, the 4H-SiC $\{10\bar{1}0\}$ becomes more stable than the $\{11\bar{2}0\}$. This preliminary research provides insight into the surface chemistry of the 4H-SiC non-polar surfaces, especially the $\{21\bar{3}0\}$, $\{31\bar{4}0\}$ and $\{32\bar{5}0\}$, which have rarely been investigated.

Introduction

Compared to standard silicon, the wide-bandgap semiconductor 4H-SiC well-known for its high electrical breakdown strength, high bulk carrier mobility, high-temperature stability and high thermal conductivity enables the realization of power devices with enhanced efficiency even under higher voltage, frequency and temperature conditions [1]. Its chemical inertness and mechanical resistance, on the one hand, render the 4H-SiC-based devices capable of operating in harsh environments but, on the other hand, results in challenges in the device fabrication process.

Etching is an important technique in the manufacturing process of power electronics. Wet etching can be an effective and low-cost method, which, in contrast to dry etching, brings little damage to the subsurface and requires less sophisticated equipment [2]. Normally, wet etching at room temperature requires external stimulation, typically through voltage bias and light irradiation.

Photoelectrochemical etching (PECE) is performed with ultraviolet (UV) light illumination and a positive voltage bias at the 4H-SiC electrode in HF or KOH solution [2-6]. The UV light illumination generates electrons and holes in the 4H-SiC, and the positive voltage pushes the holes to the interface between the electrode and electrolyte. In HF aqueous solution, which is more common and utilized in our previous research, the chemical reactions are expected to involve the carbon transforming into CO or CO_2 and the Si dissolving as SiF_6^{2-} [4-6]. Through these reactions, the PECE can effectively porosify the 4H-SiC with nanometer-sized pore structures deep into the bulk. This technology promises to optimize power device fabrication processes on cost-efficient, engineered substrates [7].

Besides the application in power electronics, porosified SiC has extensive applications in catalysis, sensors and MEMS [5, 8, 9].

The crystal structure of 4H-SiC sequentially stacks a Si and a C layer in z-direction, and commercially available wafers are normally exposed with two polar crystal surfaces (*i.e.,* Si-face and C-face) with a small tilt angle. Our previous research of PECE in HF solution has discovered that the pores etched from the C-face propagate along the [0001] direction [4, 10], as shown in Fig. 1a. The pore diameter can be easily tuned but in a limited range by varying the applied voltage with no relevant effect on the etching direction [4].

The resulting SiC porous structure will exhibit a higher surface-to-volume ratio with respect to the initial wafer implying a lasting change in its physical and chemical properties, and thus representing a remarkable platform for in-depth investigations.

Density functional theory (DFT) simulation has been extensively utilized to investigate material surface chemistry down to the atomic scale. Previous achievements of DFT in this field include the work of Dhar *et al.* revealing the termination of Si- and C-faces of 4H-SiC by simulating the interaction between HF and the last oxygen layer at the oxide/SiC interface [11].

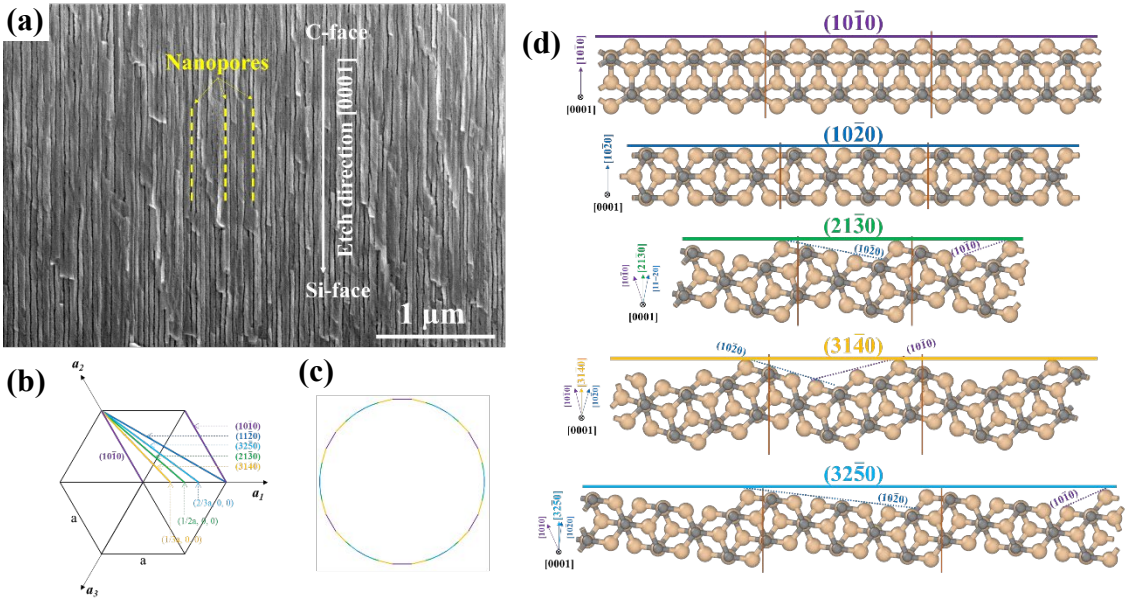

Fig. 1 (a) SEM image of cross-section view of the pores in 4H-SiC etched from C-face, (b) the expression of (10$\bar{1}$0), (11$\bar{2}$0), (21$\bar{3}$0), (31$\bar{4}$0) and (32$\bar{5}$0) in a hexagonal system, (c) pore shape by hypothesizing the equal surface energies, (d) atom structures of the five crystal planes (The structures show three supercells which are divided by the two vertical brown lines. The grey balls represent C atoms, while the yellow Si.)

The pores, etched from C-face of 4H-SiC, are along [0001] direction and thus are mainly exposed with non-polar 4H-SiC surfaces, such as {10$\bar{1}$0}, {11$\bar{2}$0}, {21$\bar{3}$0}, {31$\bar{4}$0} and {32$\bar{5}$0}. Fig. 1b shows these crystal planes in a hexagonal system. Because of hexagonal symmetry, the five crystal plane families could build a 48-gon pore wall, as shown in Fig. 1c, by utilizing Wulff's theorem and hypothesizing the equal surface energies. The 48-gon is almost a circle and can represent the pore walls. Herein, the DFT calculations are performed to investigate the surface termination of these non-polar 4H-SiC crystal planes during photoelectrochemical pore formation in the HF aqueous solution. Next, the surface energies of the ideal stoichiometric surfaces are calculated. Finally, adsorption of HF and H_2O on these surfaces is simulated to obtain the energetically favorable surface termination in HF aqueous solution. Accordingly, the surface energies of the terminated surfaces are also compared at a specific chemical potential of HF.

Computational Details

The periodic DFT calculations were performed by the plane-wave program Quantum Espresso 7.1 based on the general gradient approximation (GGA) in the form of a Perdew-Burke-Ernzerhof (PBE) functional [12]. The pseudo-potentials were chosen according to the standard solid-state pseudopotential libraries (SSSP) to represent the core electrons of each type of atom in the system [13]. The 4H-SiC primitive cell was first relaxed with cutoff energy (E_{cutoff}) of 45 Ry for the size of the plane wave basis set and a Monkhorst-Pack grid of 12 × 12 × 4 for Brillouin-zone integration. The relaxed 4H-SiC primitive cell is still in P63mc [186] symmetry with a = b = 3.095 Å, c = 10.132 Å, which is very close to the experimental results [14]. Supercells of 4H-SiC $(10\bar{1}0)$, $(11\bar{2}0)$, $(21\bar{3}0)$, $(31\bar{4}0)$ and $(32\bar{5}0)$ surfaces were built based on the relaxed primitive cell, as shown in Fig. 1d. All the atoms at the surface have at most one dangling bond, and thus the cleaved surfaces have their own most stable stoichiometric termination. One can also note that the high-index planes, i.e. $\{21\bar{3}0\}$, $\{31\bar{4}0\}$ and $\{32\bar{5}0\}$, are composed of $\{10\bar{1}0\}$ and $\{11\bar{2}0\}$ in different ratios.

The parameters of the supercells and the corresponding k-pints grids are listed in Table 1. Some atoms are fixed to simulate the bulk, while others can be relaxed to simulate the surface. As shown in Fig. 2a, b by taking 4H-SiC $(10\bar{1}0)$ as an example, for the surface energy calculation of the stoichiometric surface, the whole slab is put in the middle of the supercell in ***c***-direction and the atoms of the middle layer are fixed so that both sides can be relaxed. In contrast, only one side of the slab is simulated for the surface termination by HF and H_2O to reduce the calculation cost. Hence, the slab is at the bottom of the supercell, and the bottom-layer atoms are fixed. For adsorption energy calculation, the E_{cutoff} is increased to 55 Ry for the structures due to the requirement by the H atom, and van de Waals interaction is considered by the Grimme-D3 method [15]. Last but not least, a 20 Å vacuum layer is added in ***c***-direction to avoid the boundary effect induced by the periodic lattice.

Table 1 The parameters of supercells, k-point, E_{surf} of stoichiometric surfaces

Crystal planes	Supercell lattice [Å^3]	Atoms of supercell	Dangling bond	k-point	E_{surf} [meV/Å^2]
$(10\bar{1}0)$	12.38 × 10.13 × 37.87	112 C, 112 Si	8C, 8Si	3 × 4 × 1	179
$(11\bar{2}0)$	10.13 × 10.72 × 40.12	112 C, 112 Si	8C, 8Si	4 × 4 × 1	172
$(21\bar{3}0)$	10.13 × 8.19 × 37.90	72 C, 72 Si	6C, 6Si	4 × 5 × 1	178
$(31\bar{4}0)$	10.13 × 11.16 × 37.84	92 C, 92 Si	8C, 8Si	4 × 4 × 1	180
$(32\bar{5}0)$	10.13 × 13.49 × 35.78	104C, 104 Si	10C, 10Si	4 × 3 × 1	176

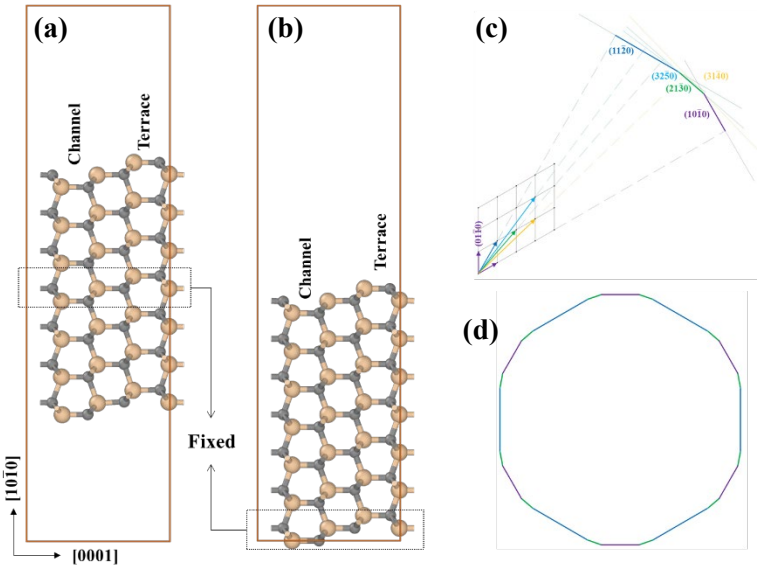

Fig. 2 Atom structures of unrelaxed 4H-SiC (10$\bar{1}$0) supercells (a) for stoichiometric surface energy calculation and (b) for surface termination simulation, (c) Wulff construction by the calculated stoichiometric surface energies and (d) the corresponding pore shape.

The surface energy (E_{surf}) per unit area is calculated by Eq. 1

$$E_{surf} = (E_{slab1} - \mathrm{N} \times E_{cell}) / (2 \times \mathrm{A}), \quad (1)$$

where E_{slab1} is the energy of the two-side relaxed slab, N the number of primitive cells in the slab and E_{cell} is the energy of the 4H-SiC primitive cell. The adsorption energy (E_{ads}) of each single molecule is by Eq. 2

$$E_{ads} = (E_{slab2\_n\ molecules} - E_{slab2} - \mathrm{n} \times E_{molecule}) / \mathrm{n}, \quad (2)$$

where $E_{slab2\_n\ molecules}$ is the energy of the one-side relaxed slab together with the n number of molecules adsorbed, and E_{slab2} and $E_{molecule}$ is the energy of the slab and the molecule, respectively.

Results and Discussions

The E_{surf} of the five crystal planes are listed in Table 1. For the stoichiometric surfaces, the 4H-SiC {11$\bar{2}$0} is the most stable non-polar crystal plane, followed by {32$\bar{5}$0}, {21$\bar{3}$0}, {10$\bar{1}$0} and {31$\bar{4}$0}. Rauls *et al.* have also reported that the surface energy of the (11$\bar{2}$0) is lower than that of the (10$\bar{1}$0) [16]. Based on these surface energies, the pore shape can be constructed by Wulff's theorem (Fig. 2c, d) [17]. Naturally, the surfaces cannot be clean in the HF aqueous solution. High temperature annealing in the inert atmosphere, for example helium, can result in a clean surface and allow the pore to reorganize into the equilibrium shape. However, the surface history of the pore walls, *i.e.* the terminations, must influence on the reorganization. To explain the behaviors of the pore during annealing, there is a need to understand the terminations of the pore walls during PECE.

All the 4H-SiC surfaces of the pore wall are highly affinitive to the HF and H_2O molecules in the etching solution. Fig. 3 shows the adsorption configurations of a single HF or H_2O molecule on the 4H-SiC (10$\bar{1}$0) and (11$\bar{2}$0) surfaces. On the 4H-SiC (10$\bar{1}$0) are terrace and channel sites (Fig. 3a-d), which one can easily identify in Fig. 2a, b. The HF molecule can be dissociatively adsorbed at both sites with F boding to Si and H to C (Fig. 3a, b). The E_{ads} at the terrace and channel sites are −4.36 and −4.78 eV. For H_2O, the terrace site only allows the molecular adsorption with the O bonding to Si (Fig. 3c) and E_{ads} of −0.73 eV, and the channel site makes the dissociative adsorption of H_2O favorable with E_{ads} of −4.36 eV (Fig. 3d). The reason for the high E_{ads} at the channel site is that the two dangling bonds of the pair of the Si and C at the channel point towards each other, which allows the hydrogen bond interaction between H and the F (or O) after the dissociation of HF (or H_2O).

There is not much difference for the sites on the $\{11\bar{2}0\}$ surface, where HF and H_2O can be dissociatively adsorbed with E_{ads} values of −3.65 and −3.09 eV (Fig. 3e, f).

Since the 4H-SiC $\{21\bar{3}0\}$, $\{31\bar{4}0\}$ and $\{32\bar{5}0\}$ possess the same sites as those on the 4H-SiC $\{10\bar{1}0\}$ and $\{11\bar{2}0\}$, all of them render the dissociative adsorption of HF and H_2O. Additionally, they have the corner sites, as indicated in Fig. 2d, whereas the corner sites do not facilitate the adsorption. The E_{ads} of a single HF and H_2O molecule on these non-polar crystal planes are listed in Table 2. The former ranges from −3.87 to −4.78 eV, and the latter from −3.12 to −4.36 eV. All these surfaces are more affinitive to HF.

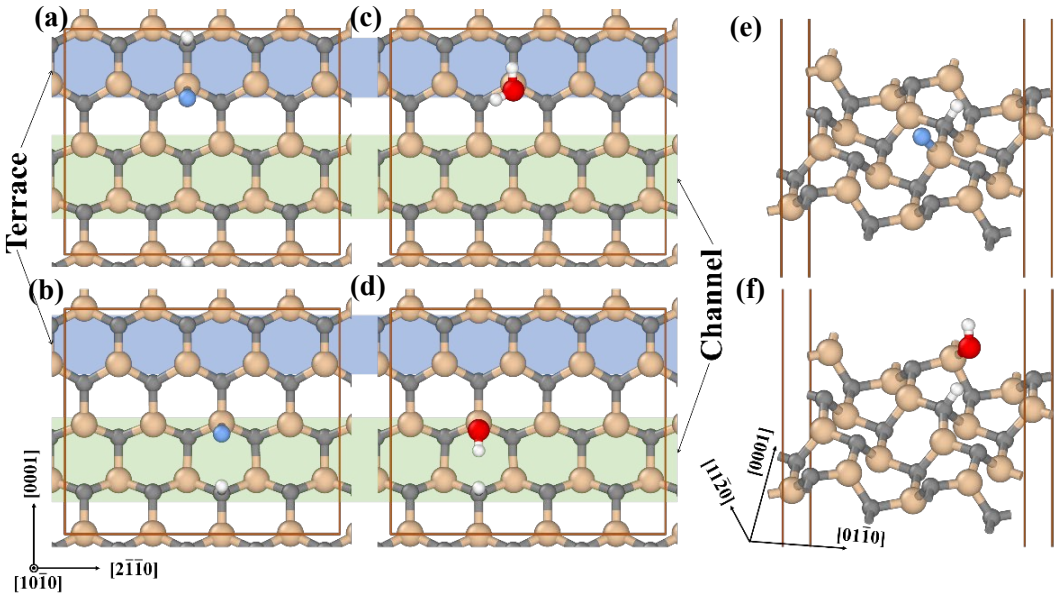

Fig. 3 Atom configurations. (a, b) A single HF and (c, d) a single H_2O adsorbed on the terrace and channel site of the 4H-SiC $(10\bar{1}0)$, and (e) A single HF and (f) a single H_2O adsorbed on the 4H-SiC $(11\bar{2}0)$. (The white balls are the H atoms, the red O and the blue F.)

The high affinity of HF can make the surface completely terminated only with HF, *i.e.* all the dangling Si and C bonds are replaced with the F and the H. The full layer adsorption of HF on the 4H-SiC $(10\bar{1}0)$ and $(11\bar{2}0)$ surfaces are shown Fig. 4a, b. The average E_{ads} of each molecule on these five surfaces is still very high (−3.85 ~ −4.21 eV), as listed in Table 2. The 4H-SiC $(10\bar{1}0)$ shows the highest E_{ads} per HF but the lowest E_{ads} per unit area. By adding the E_{ads} per unit area to the E_{surf} of the stoichiometric crystal planes, the E_{surf} of the terminated crystal planes can be obtained (Last column of Table 2). All of them are negative values, suggesting that the 4H-SiC can be dissolved by HF at high HF chemical potential [18]. The calculated reaction energy of $SiC + 4HF \rightarrow SiF_4 + CH_4$ is −4.22 eV. This reaction has been identified and its reverse reaction has been utilized to deposit SiC film with SiF_4-CH_4 plasma [19, 20]. The high affinity of HF on the surface originates from the high strength of Si-F (582 kJ/mol) and C-H bond (416 kJ/mol)) [19].

As mentioned, the E_{ads} of the HF is calculated by Eq. 2 with $E_{molecule}$ being the energy of a single HF molecule. However, the value of E_{ads} is related to the chemical potential of each element or each composition in the practical system [21]. The Eq. 2 is very close to a system with a high HF chemical potential, such as a pure HF gas phase at high temperature. In the HF aqueous solution for PECE the HF chemical potential should be much lower. By setting the chemical potential of a single HF molecule as zero, the E_{surf} of the terminated crystal planes can be obtained at the lower HF chemical potential, as shown in Fig. 4c. With the decrease of HF chemical potential, the fully covered surfaces increase their E_{surf} and thus become less stable. Hence, in a diluent HF aqueous solution, some HF could be replaced with H_2O molecule by considering that the surfaces also have high chemical affinity to H_2O.

Table 2 The E_{ads} values of HF and H_2O and the E_{surf} of the completely terminated crystal planes.

Crystal planes	[a]E_{ads} [eV]			[b]E_{ads} [meV/Å^2]	[c]E_{surf} [meV/Å^2]
	HF	H_2O	Comp. HF	Comp. HF	Comp. HF
$(10\bar{1}0)$	−4.78	−4.36	−4.21	−267	−90
$(11\bar{2}0)$	−3.65	−3.09	−3.78	−279	−106
$(21\bar{3}0)$	−4.48	−3.45	−3.89	−282	−104
$(31\bar{4}0)$	−4.70	−4.21	−3.93	−278	−98
$(32\bar{5}0)$	−3.87	−3.12	−3.85	−282	−105

Note: [a]E_{ads} means the E_{ads} of each single molecule, [b]E_{ads} the E_{ads} per unit area, and [c]E_{surf} the E_{surf} of the HF terminated crystal planes with respect to the chemical potential of a single HF molecule. The value of the last column is the intersection in Fig. 4c.

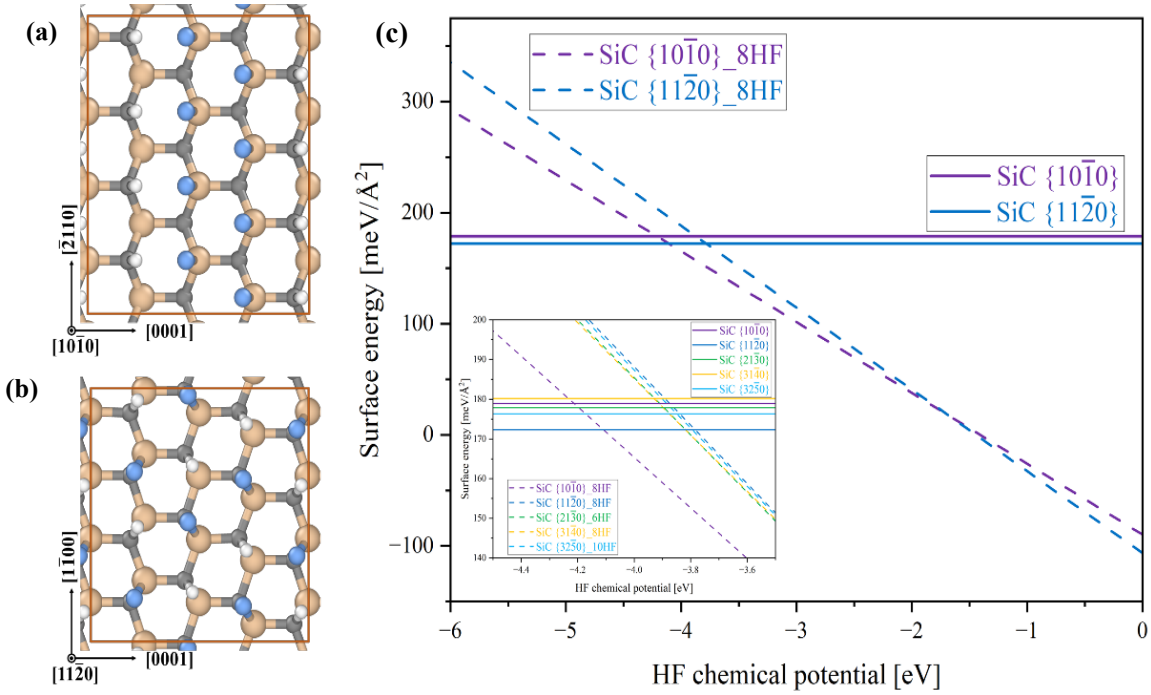

Fig. 4 Atom configurations of a full-layer HF adsorption on the 4H-SiC (a) $(10\bar{1}0)$ and (b) $(11\bar{2}0)$, (c) the E_{surf} of the crystal planes with respect to HF chemical potential which is set the potential of a single HF molecule as zero. The slope is (1000 × n) / A, where n is the number of the adsorbed HF molecule and A is the surface area.

Another significant point shown in Fig. 4c is that the stability order of the crystal planes can be changed by the HF adsorption. The stoichiometric 4H-SiC $\{10\bar{1}0\}$ is less stable than $\{11\bar{2}0\}$, whereas in the range of HF chemical potential from −4.10 to −1.70 eV the 4H-SiC $\{10\bar{1}0\}$ becomes more stable.

Summary and Outlook

In this work, we simulate the terminations of five 4H-SiC non-polar surfaces, *i.e.* $\{10\bar{1}0\}$, $\{11\bar{2}0\}$, $\{21\bar{3}0\}$, $\{31\bar{4}0\}$ and $\{32\bar{5}0\}$, which can well represent the walls of the C-face etched pores penetrating in [0001] direction. The E_{surf} of the stoichiometric surfaces are calculated, with the sequence of $\{11\bar{2}0\} < \{32\bar{5}0\} < \{21\bar{3}0\} < \{10\bar{1}0\} < \{31\bar{4}0\}$. Adsorption of a single HF or H_2O molecule on the surfaces are also calculated, and the results demonstrate that all the surfaces are more affinitive to HF than H_2O. Accordingly, we simulate the surfaces completely terminated with HF and obtain their relative stability with respect to the HF chemical potential.

This preliminary research provides some insight into the surface chemistry of the 4H-SiC non-polar surfaces among which the $\{21\bar{3}0\}$, $\{31\bar{4}0\}$ and $\{32\bar{5}0\}$ have rarely been investigated. However, our simulation is somehow an idealistic case where these stoichiometric crystal planes are hypothesized to be created under an ultra-clean condition and then directly immersed into the HF aqueous solution. The practical surface terminations are expected to be more complicated and should be influenced by the etching mechanism, which is still under study whether the 4H-SiC is directly dissolved by HF or it is firstly oxidized into SiO_2 by H_2O and then dissolved HF. This research understanding of surface chemistry helps to reveal the etching mechanism. In the near future, the surface reaction of HF and H_2O on these 4H-SiC crystal planes will be simulated.

Acknowledgements

The financial support by the Austrian Federal Ministry of Labour and Economy, the National Foundation for Research, Technology and Development and the Christian Doppler Research Association is gratefully acknowledged. We also acknowledge the computation resource from the Vienna Scientific Cluster (VSC-5).

References

[1] X. Yuan, I. Laird, S. Walder, Opportunities, challenges, and potential solutions in the application of fast-switching SiC power devices and converters, IEEE Trans. Power Electron. 36 (2021) 3925-3945.

[2] K. Mairhofer, S. Larisegger, A. Foelske, M. Sauer, G. Friedbacher, G. Fafilek, New insights into the photoassisted anodic reactions of n-type 4H SiC semiconductors, Monatsh. Chemie 155 (2024) 683-696.

[3] S. Whiteley, A. Sorensen, J. J. Vajo, R. Sfadia, T. D. Ladd, S. Cui, J. Graetz, Dopant selective photoelectrochemical etching of SiC, J. Electrochem. Soc. 170 (2023) 036508.

[4] M. Leitgeb, G. Pfusterschmied, S. Schwarz, B. Depuydt, J. Cho, U. Schmid, Communication-current oscillations in photoelectrochemical etching of monocrystalline 4H silicon carbide, ECS J. Solid State Sci. Technol. 10 (2021) 073003.

[5] M. Leitgeb, C. Zellner, M. Schneider, U. Schmid, Porous single crystalline 4H silicon carbide rugate mirrors APL Mater. 5 (2017) 106106.

[6] M. Leitgeb, C. Zellner, C. Hufnagl, M. Schneider, S. Schwab, H. Hutter, U. Schmid, Stacked layers of different porosity in 4H SiC substrates applying a photoelectrochemical approach, J. Electrochem. Soc. 164 (2017) E337.

[7] C. S. Solanki, R. R. Bilyalov, J. Poortmans, J. Nijs, R. Mertens, Porous silicon layer transfer processes for solar cells, Sol. Energ. Mater. Sol. C. 83 (2004) 101-113.

[8] M. Xu, Y. R. Girish, P. Wu, H. M. Manukumar, S. M. Byrappa, Udayabhanu, K. Byrappa, Recent advances and challenges in silicon carbide (SiC) ceramic nanoarchitectures and their applications, Mater. Today Commun. 28 (2021) 102533.

[9] G. Tuci, Y. Liu, A. Rossin, X. Guo, C. Pham, G. Giambastiani, C. Pham-Huu, Porous silicon carbide (SiC): a chance for improving catalysts or just another active-phase carrier? Chem. Rev. 121 (2021) 10559-10665.

[10] M. Leitgeb, C. Zellner, M. Schneider, U. Schmid, A combination of metal assisted photochemical and photoelectrochemical etching for tailored porosification of 4H SiC substrates, ECS J. Solid State Sci. Technol. 5 (2016) P556.

[11] S. Dhar, O. Seitz, M. D. Halls, S. Choi, Y. J. Chabal, L. C. Feldman, Chemical properties of xxidized silicon carbide surfaces upon etching in hydrofluoric acid, J. Am. Chem. Soc. 131 (2009) 16808-16813.

[12] P. Giannozz, S. Baroni, N. Bonini, M. Calandra, R. Car, C. Cavazzoni, D. Ceresoli, G. L. Chiarotti, M. Cococcioni, I. Dabo, *et al.*, QUANTUM ESPRESSO: a modular and open-source software project for quantum simulations of materials, J. Phys.: Condens. Matter 21 (2009) 395502.

[13] G. Prandini, A. Marrazzo, I. E. Castelli, N. Mounet, N. Marzari, Precision and efficiency in solid-state pseudopotential calculations, Npj Comput. Mater. 4 (2018) 72.

[14] A. L. Hannam and P. T. B. Shaffer, Revised X-ray diffraction line intensities for silicon carbide polytypes, J. Appl. Crystallogr. 2 (1969) 45-48.

[15] S. Grimme, J. Antony, S. Ehrlich, H. Krieg, A consistent and accurate ab initio parametrization of density functional dispersion correction (DFT-D) for the 94 elements H-Pu, J. Chem. Phys. 132 (2010) 154104.

[16] E. Rauls, Z. Hajnal, P. Deák, T. Frauenheim, Theoretical study of the nonpolar surfaces and their oxygen passivation in 4H- 6H-SiC, Phys. Rev. B 64 (2001) 245323.

[17] G. Wulff, On the question of speed of growth and dissolution of crystal surfaces, Z. Kristallogr, 34 (1901) 449.

[18] X.-G. Wang, A. Chaka, M. Scheffler, Effect of the environment on alpha-Al_2O_3 (0001) surface structures, Phys. Rev. Lett. 84 (2000) 3650-3653.

[19] G. Cicala, P. Capezzuto, G. Bruno, M. C. Rossi, Growth chemistry of SiC alloys from SiF_4-CH_4 plasmas, Appl. Surf. Sci. 184 (2001) 66-71.

[20] H. Suzuki, H. Araki, M. Tosa, T. Noda, SiC film formation from fluorosilane gas by plasma CVD, J. Cryst. Growth 294 (2006) 464-468.

[21] K. Reuter, M. Scheffler, Composition, structure, and stability of RuO_2 (110) as a function of oxygen pressure, Phys. Rev. B 65 (2001) 035406.